

Sub-60 mV/decade switching with a cold metal as the injection source

Fei Liu^{1,*}

*¹Institute of Microelectronics and Key Laboratory
of Microelectronics Devices and Circuits (MoE),
Peking University, Beijing 100871, China*

Abstract

Power dissipation is a great challenge for the continuous scaling down and performance improvement of CMOS technology, due to thermionic current switching limit of conventional MOSFETs. In this work, we show that this problem can be overcome by using cold metals as the transistor's injection source, which are different from conventional metals and can filter high energy electrons to break the Boltzmann tyranny. It is proved that the subthreshold swing (SS) of thermionic current of transistor using cold metal contact can be extremely smaller than 60 mV/decade at room temperature. Specifically, two-dimensional (2D) transition metal chalcogenide (TMD) cold metals of NbX₂ and TaX₂ (X=S, Se, Te) are proposed as the injection source of FETs. Quantum transport simulations indicate that promising switching efficiency and on-state current can be achieved using TMD cold metal injection source, which is beneficial for energy efficient applications.

KEYWORDS: Cold metal, energy efficient, subthreshold swing, quantum transport simulations, two dimensional materials

INTRODUCTION

The power consumption becomes increasingly severe with the improvement of integration degree, and becomes an important bottleneck for the advancement of CMOS technology along Moore's law[1, 2]. High power consumption will not only increase chip temperature and failure rate, but also increase chip design, packaging and cooling costs. Especially with the rise of various mobile electronic devices, such as smart phones, wearable devices, internet of things, etc. The demand for reducing chip power consumption is increasingly strong. Both the static and dynamic power consumption of the chip is related to the supply voltage, so lowering the supply voltage is an effective way to reduce the power consumption of the chip[1, 2]. However, this is subject to the transistor subthreshold swing (SS) limit, which cannot be lower than 60 mV/decade at room temperature.

Steep slope devices have attracted much attention for designing power-constrained applications by using tunneling[3, 4], impact ionization[5] and negative capacitance[6]. Recently, cold source FETs (CS-FETs) are proposed to obtain the sub-thermionic switching by source density of states (DOS) engineering cutting-off the Boltzmann tail of the current[7]. Such cold source can be realized by using emerging Dirac materials[8, 9], properly doped semiconductors[7, 8] or a narrow-energy conduction band of dangling bonds[10]. However, these proposed cold source requires properly doping and heterogenous integration. An ideal solution is to find a kind of cold metals to replace conventional metals as the contact of transistors. Such cold metals would filter high energy electrons in the subthreshold region.

In this work, an emerging steep slope device using cold metal contact is proposed. Here, cold metals are applied to replace conventional metals as the FET contact. Different from conventional metals, cold metals have an energy gap around the Fermi level and work like p-type or n-type doped semiconductors. Therefore, electron in the energy region can be effectively filtered, which results in sub-60 mV/decade switching. As the emergence of 2D materials, such metallic materials with required properties can be found in monolayer (ML) NbX_2 and TaX_2 ($X = \text{S}, \text{Se}, \text{Te}$), which be achieved by mechanical exfoliation[11, 12], chemical exfoliation[13–15] or chemical vapour deposition method (CVD)[16–20]. We investigated 2D heterojunction CS-FETs using cold metal contact of metallic transition metal dichalcogenides (TMDs) as the injection source by quantum transport simulations using the non-equilibrium Greens function (NEGF) formalism. It is demonstrated that CS-

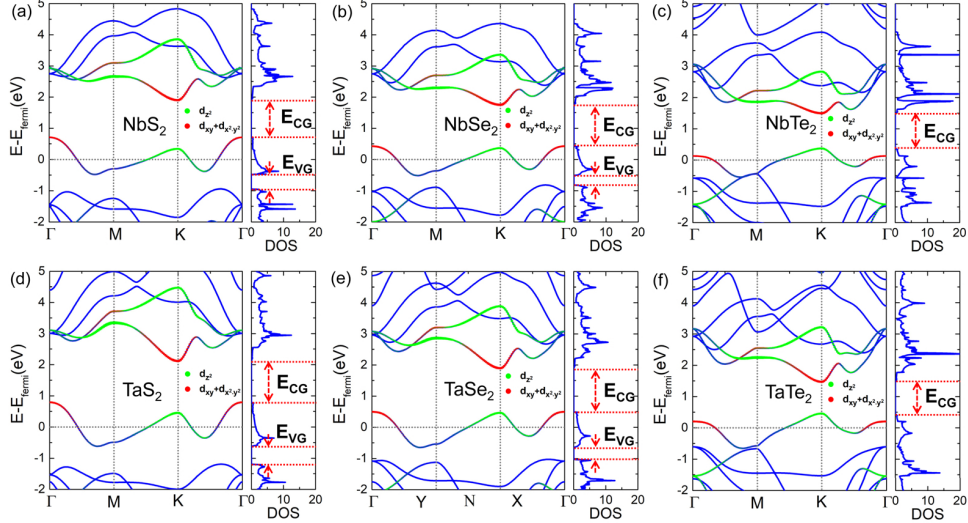


FIG. 1: Band structures for monolayer metallic MX_2 ($M = \text{Nb}, \text{Ta}$; $X = \text{S}, \text{Se}, \text{Te}$). Fermi energy is set to zero. Different from conventional metals, there is an energy gap in the conduction band (E_{CG}) or valence band (E_{VG}). Therefore, electron in the gap can be filtered as these metallic materials are applied as the transistor's injection source.

FETs with TMD cold metal contacts have promising device performance of energy efficient switching and high on-state current. Our work reveals a novel design rule for future steep slope electronic devices using cold metal contact.

RESULTS AND DISCUSSION

Cold metals Metals widely exist in nature and are a very important substance for the semiconductor industry. In MOSFETs, metallic materials are applied as the contacts, gates and interconnects. Usually, these bulk metals have excellent electrical conductivity with continuous DOS around the Fermi level. Recently, 2D metallic materials have been intensively investigated due to their exotic properties[21]. When reducing the dimension from bulk metallic TMDs to atomic thin limit, 2H-NbSe₂ has been found to exhibit intriguing quantum phenomena of superconductivity and charge density wave[12, 22–24]. Monolayer 2H-NbS₂ has been synthesized epitaxially and applied as the injection source of 2D FETs using the lateral and vertical NbS₂-WS₂ heterostructures[20].

Here, we first investigated electronic properties of metallic TMDs by the density functional theory (DFT) calculations, which were performed using the Vienna ab initio sim-

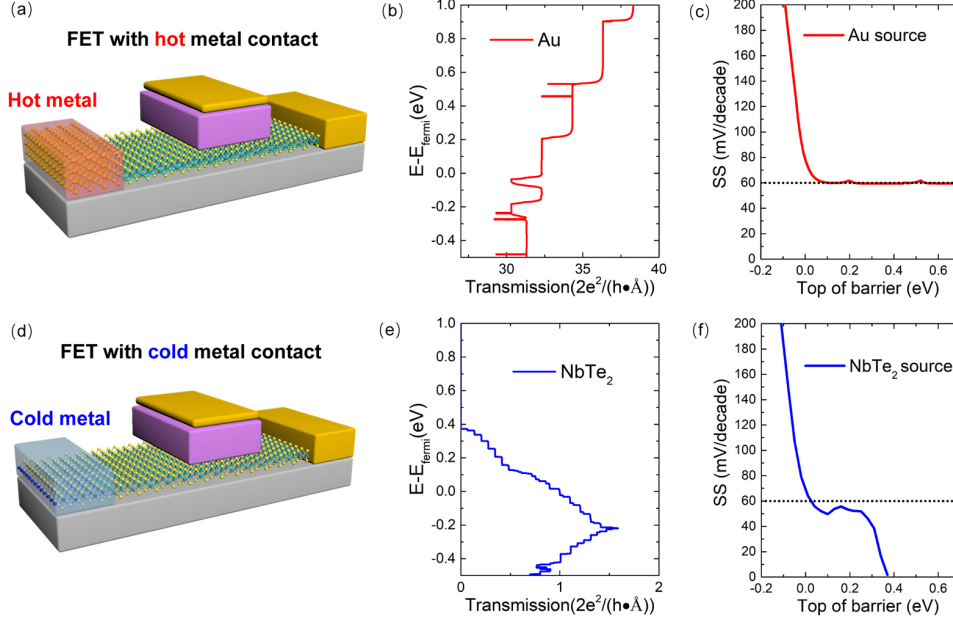


FIG. 2: Comparison between conventional hot metal and cold metal contacts for transistors. Schematic illustration of transistors with (a) hot and (d) cold metals. Conventional metal of Au have a continuous transport channel around the Fermi level (b), while cold metal of NbTe₂ have an energy region without channel above the Fermi level(e). Subthreshold swing of transistor using Au is always larger than 60 mV/decade (c), while SS using NbTe₂ as the injection source can break the thermionic limit (f).

ulation package (VASP)[25]. The core-valence interaction was described by the projector augmented wave (PAW) method[26, 27]. Exchange-correlation functional of metallic TMDs was described by the generalized gradient approximation of Perdew-Burke-Ernzerhof (GGA-PBE)[28, 29]. While, the band structure calculations of semiconducting TMDs were performed by using the Heyd-Scuseria-Ernzerhof (HSE06) hybrid functional[30, 31]. Energy cut off for plane-wave expansion was set to 500 eV. Monkhorst-Pack (MP) k point meshes were used for Brillouin zone sampling with a grid of $15 \times 15 \times 1$ for both structure relaxations and self-consistent calculations. Atomic structures were relaxed until the calculated residual forces are smaller than $0.01 \text{ eV}/\text{\AA}$. A vacuum layer larger than 15 \AA is used to avoid adjacent image interaction.

As one kind of TMDs, 2H-NbX_2 ($X = \text{S, Se, Te}$) has a common chemical formula of MX_2 with a transition-metal layer atoms sandwiched between two layers of chalcogen X atoms with covalent bonds. It is well known that 2H-MoX_2 are semiconducting with the lowest

subbands contributed by the d_{z^2} , d_{xy} , and $d_{x^2-y^2}$ orbitals of transition-metal atoms. There are 5 d electrons in the 4-th shell and the valence bands are filled. However, Nb atoms have one less d electron in the outermost shell and the Fermi level is in the valence bands. 2H-NbX₂ are metallic and the band structures of 2H-NbX₂ have similar shapes as those of MoX₂ as shown in Fig. 1. The single band around the Fermi level is contributed by the hybridization of the d_{z^2} , d_{xy} , and $d_{x^2-y^2}$ orbitals. Similarly, 2H-TaX₂ are also metallic and have similar band structures with the Fermi level across the topmost valence band. Unlike conventional metals with continuous density of states around the Fermi level, there is an energy gap above the chemical potential of these materials as shown in Fig. 1. At the same time, a valence band gap appears below the Fermi level of NbS₂, NbSe₂, TaS₂ and TaSe₂. Therefore, these metallic materials are naturally p-type or n-type semiconductor without artificial doping. When these metallic materials are applied as the injection source of FETs, electrons with energy in the gap can be filtered.

Next, we compared the difference between 2H-NbX₂ and traditional metal as the FET contact. Fig. 2 (a) and (d) shows the schematic device structures with Au and 2H-NbTe₂ as the injection source, respectively. The current through the device can be calculated by the Landauer-Buttiker formula[32]:

$$I_D = \frac{2q}{h} \int T(E)[f_S - f_D]dE \quad (1)$$

Where $T(E)$ is the transmission coefficient, f_S and f_D are the Fermi functions of the source and drain, respectively. Fig. 2(b) plots the transmission as a function of energy of 3 nm golden film, which is calculated by using NEGF-DFT implemented in Nanodcal[33]. As expected, golden film have a continuous transport channel around the Fermi level of $E_F = 0$ eV. In contrast, Fig. 2(e) shows that there is no transport channel above due to the energy gap in the conduction band of 2H-NbTe₂. The SS is given by [1, 2]:

$$SS = \frac{\partial V_G}{\partial \log_{10}(I_D)} \quad (2)$$

where V_G is the gate voltage. In the case of neglecting the tunneling current, the SS of thermionic current as a function of the top of channel barrier is calculated using the obtained transmission of Au contact in Fig. 2(c). Here, the top of barrier is modulated by the gate voltage. It can be found that the SS can not break the switching limit of 60 mV/decade using Au contact. Differently, 2H-NbTe₂ has an energy gap in the conduction band (E_{CG}).

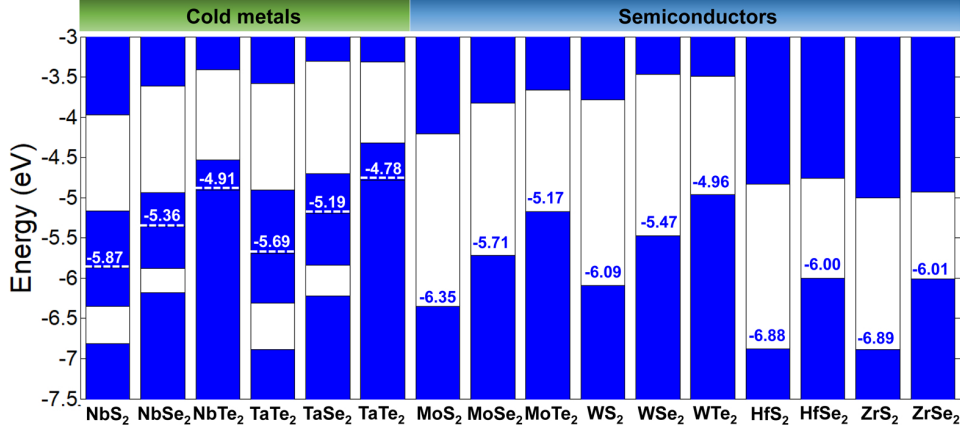


FIG. 3: Calculated band alignment for metallic and semiconducting TMDs. Schottky and Ohmic contacts can be realized by properly choosing metallic and semiconducting TMDs.

When the top of barrier is in the E_{CG} , the current does not change as the lowering of channel barrier and SS is infinitely large. While, as the top of barrier gets smaller than $E = 0.37$ eV, the current is suddenly increased and SS is extremely small as shown in Fig. 2 (f). It is also found that the SS keeps smaller than 60 mV/decade in the energy region of due to the linearly increased channels, which is beneficial for the energy efficient switching. The physics behind this sub-60 mV/decade using 2H-NbTe₂ is that the high energy electron above the Fermi level is filtered by the energy gap. Hence, the off-state current does not change when the top of barrier is in the energy gap region. 2H-NbTe₂ as the FET injection source is different from conventional metal and works like a cold source by filtering high energy electrons to realize sub-60 mV/decade switching.

Band offsets of metals and semiconductors are essential for device design. Therefore, we studied band alignments of metallic and semiconducting TMDs by the first principles calculations using VASP as shown in Fig. 3. Here, NbX₂, TaX₂, MoX₂ and WX₂ are in 2H-phase while HfX₂ and ZrX₂ are in 1T phase[34]. As the atomic number of X increases (from S to Te), the Fermi level of NbX₂ increases. The Fermi levels of TaX₂ are higher than those of NbX₂ due to much higher energy of the 5d orbital of the transition metal. It can be found that the contact between metallic and semiconducting TMDs is a Schottky type for the same X, such as NbS₂-MoS₂ and NbTe₂-MoTe₂. NbS₂ has the lowest fermi level and is much easier to realize p-type Ohmic contact, such as NbS₂-MoSe₂ and NbS₂-WS₂. In contrast, TaTe₂ has the highest chemical potential and can be applied as n-type Ohmic

contact, such as TaTe₂-ZrS₂ and TaTe₂-HfS₂.

Steep slope FETs with cold metal contact To assess the role of cold metals of metallic TMDs as the injection source, we constructed hetero-junction FETs using TMDs. It has been shown that metallic NbX₂ can be exfoliated from bulk counterpart[11, 12] or synthesized by a chemical vapor deposition (CVD) method[20]. Moreover, both lateral and vertical metal-semiconductor NbS₂-WS₂ hetero-structures are achieved[20], which paves a promising way to construct CS-FETs using 2D metal-semiconductor TMD hetero-junctions. An important metric for choosing proper cold metal for n-type FET is the energy difference between the Fermi level and band gap in conduction band, which is 0.71 eV, 0.42 eV and 0.37 eV for 2H-NbS₂, 2H-NbSe₂ and 2H-NbTe₂, respectively. The energy difference can not be too large in order to filter those electrons in sub-threshold region. So, 2H-NbTe₂ is applied as the injection source and MoSe₂ is used as the channel material of CS-FETs as shown in Fig. 4(a). The two materials have relatively small lattice mismatching. According to the band alignments, the contact between NbTe₂ and MoSe₂ is a Schottky type and the n-type Schottky barrier is 1.08 eV as shown in Fig. 3. To reduce the Schottky barrier, 5% compressive strain and 5% tensile strain are applied on NbTe₂ and MoSe₂, respectively. As a result, the n-type Schottky barrier is reduced to 0.09 eV.

The transfer characteristics (I_D - V_G) of CS-FETs and MoSe₂ FETs are compared at $V_D = 0.5$ V in Fig. 4(d). High dielectric material of 3 nm HfO₂ is applied as the top and bottom oxides. The source, drain and gate lengths of simulated FETs are 15 nm, 15 nm and 10 nm, respectively. Metallic NbTe₂ is 4 nm in the source of NbTe₂-MoSe₂ CS-FETs. Three band tight binding model is applied to describe 2H-NbTe₂ and 2H-MoSe₂[35], and MoSe₂ in the source and drain regions is doped to n-type. Device performance calculations are performed by self-consistently solving the Poisson equation and Schrodinger equation within the NEGF formalism[36]. The Off-current is fixed to 10 pA/ μ m at $V_G = 0$ V. Compared with MoSe₂ FETs, device performance is improved in NbTe₂-MoSe₂ CS-FETs. On-current of CS-FETs reaches $4.4 \times 10^2 \mu A/\mu m$ larger than $3.4 \times 10^2 \mu A/\mu m$ MoSe₂ -FETs. The SS of CS-FETs is about 51 mV/decade between $0.0 \text{ V} < V_G < 0.1 \text{ V}$, while the SS of MoSe₂ FETs is around 65 mV/decade. Even though the SS of CS-FETs breaks the switching limit, it is much larger than theoretical prediction in Fig. 3. The reason is that the band gap edge in conduction band of 2H-NbTe₂ under -5% strain is 0.41 eV and electrons for deep subthreshold region are filtered rather than those for subthreshold region with current larger

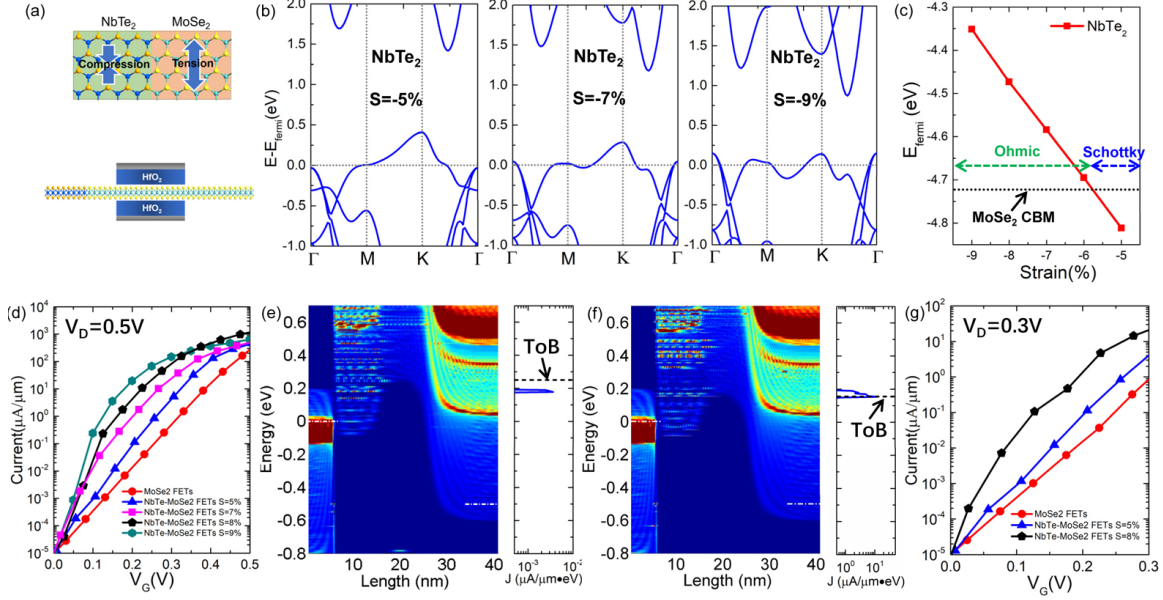


FIG. 4: Structure and performance of NbTe₂-MoSe₂ CS-FETs. (a) Schematic device structure of hetero-junction CS-FETs using NbTe₂ and MoSe₂. (b) Band structures of NbTe₂ under compressive strain. (c) The Fermi energy of NbTe₂ as a function of strain. Under compressive strain, the contact type between NbTe₂ and MoSe₂ changes from Schottky contact to Ohmic contact. (d) I_D - V_G of NbTe₂-MoSe₂ CS-FETs with NbTe₂ under compressive strain at $V_D = 0.5$ V. Device performance can be improved by the strain. Local density of states of NbTe₂-MoSe₂ CS-FETs with -8% strain on NbTe₂ with top of barrier (ToB) (e) above ($V_G = -0.03$ V) and (f) below ($V_G = -0.13$ V) source valence band maximum (VBM). (g) I_D - V_G of NbTe₂-MoSe₂ CS-FETs with NbTe₂ at $V_D = 0.3$ V.

than 10^{-5} $\mu\text{A}/\mu\text{m}$. Therefore, the VBM of 2H-NbTe₂ has to be reduced in order to improve the device performance of NbTe₂-MoS₂ CS-FETs.

Fig. 4(b) shows the band structure of NbTe₂ under compressive strain. As the compressive strain is increased from 5% to 9%, the energy difference between the Fermi level and VBM is decreased from 0.41 eV to 0.15 eV. The strain also changes the Fermi level of NbTe₂ as shown in Fig. 4(c). The Fermi energy increased with the compressive strain, so the contact between NbTe₂ and MoSe₂ changes from Schottky type at $S = -5\%$ to Ohmic type at $S = -9\%$. Fig. 4(d) shows that current switching is greatly improved in NbTe₂-MoS₂ CS-FETs as the increasing of compressive strain on NbTe₂. SS is as small as 26 and 23 mV/decade under 8% and 9% compressive strain on NbTe₂, respectively. Fig. 4 (e) plots the local DOS (LDOS) along the channel at $V_G = 0.03$ V with -8% strain on NbTe₂. The

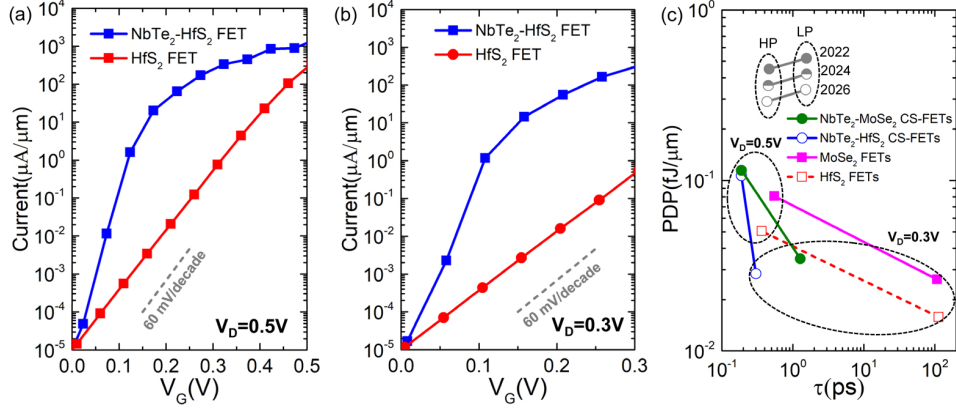


FIG. 5: Device performance of NbTe₂-HfS₂ CS-FETs. I_D - V_G of NbTe₂-HfS₂ CS-FETs and HfS₂ FETs at (a) $V_G = 0.5$ V and (b) $V_G = 0.3$ V. Power-delay product and switching speed of NbTe₂-MoSe₂ CS-FETs, NbTe₂-HfS₂ CS-FETs, MoSe₂ FETs and HfS₂ FETs compared with the requirements of the ITRS 2013[37].

top of channel barrier is above the VBM of NbTe₂ and current is composed of 100% direct tunneling current from source to drain in Fig. 4(e). As the gate voltage is increased to $V_G = 0.13$ V, the ToB gets lower than the source VBM in Fig. 4(f). As a result, the current is mainly thermionic current over the channel barrier. I_{on} can be as large as $1.2 \times 10^3 \mu\text{A}/\mu\text{m}$, which is larger than $5.3 \times 10^2 \mu\text{A}/\mu\text{m}$ of the low power requirements of the International Technology Roadmap for Semiconductors (ITRS) 2013[37] for $L_g = 10$ nm at $V_D = 0.75$ V. Advantages of CS-FET gets more significant as V_D is scaled to 0.3 V as shown in Fig. 4(g). I_{on} reaches $23 \mu\text{A}/\mu\text{m}$ over ten times larger than that of MoSe₂ FETs and I_{on}/I_{off} ratio is over 10^6 .

We also constructed NbTe₂-HfS₂ CS-FETs because the contact between the two materials is intrinsically Ohmic type as shown in Fig. 3. At the same time, lattice mismatching between ML-NbTe₂ and ML-HfS₂ is tiny. ML-NbTe₂ is under -9% biaxial strain and ML-HfS₂ is applied as the channel material. Both ML-NbTe₂ and ML-HfS₂ are described by eleven band tight-binding model[38] based on maximally localized Wannier functions[39, 40]. Due to the Ohmic contact, device performance of NbTe₂-HfS₂ CS-FETs is promising and much better than that of HfS₂ FETs as shown in Fig. 5(a, b). I_{on} reaches $1.2 \times 10^3 \mu\text{A}/\mu\text{m}$ and $3.1 \times 10^2 \mu\text{A}/\mu\text{m}$ at $V_D = 0.5$ V and 0.3 V, respectively. We also investigated the switching speed and energy efficiency of NbTe₂-MoSe₂ and NbTe₂-MoSe₂ CS-FETs in Fig. 5(c). The switching speed is measured by the intrinsic delay, defined as $\tau = (Q_{on} - Q_{off})/I_{on}$,

where $Q_{on/off}$ is the channel total charge in the on/off state. Energy efficiency is measured by power-delay product (PDP) given by $PDP = V_D(Q_{on} - Q_{off})$. It can be found that switching speeds and switching energies of NbTe₂-MoSe₂ and NbTe₂-HfS₂ CS-FETs at $L_G = 10$ nm and $V_D = 0.5$ V are much better than the requirements of the ITRS 2013[37]. For example, the switching speed of NbTe₂-HfS₂ CS-FETs is 2.4 and 8.3 times faster than the requirement of ITRS 2013 for high-performance (HP) and low-power (LP) applications, respectively. While, the PDP is only 24% and 21% for HP and LP applications, respectively. As the supply voltage is decreased to 0.3 V, PDP and switching speed can be further improved while on-state current is decreased. MoSe₂ FETs and HfS₂ FETs also have lower PDP but the on-state currents are much smaller than those of CS-FETs, which also results in longer switching speed.

At last, we discussed the possible magnetic state of NbTe₂ which may have significant impact on realizing sub-60 mV/decade switching using such cold metal. The transition metals of Nb and Ta have one unpaired outmost electron, so magnetic moment may appear. It has been shown that intrinsic NbX₂ has no magnetic moment, while NbS₂ and NbSe₂ structures can be magnetized under tensile strain[41]. It is predicted that NbS₂ and NbSe₂ under 10% tensile strain are ferromagnetic room temperature. Here, we applied NbTe₂ under compressive strain as the contact. The energy difference per unit cell between ferromagnetic and anti-ferromagnetic NbTe₂ under -9% strain is 30 mV. The Curie temperature T_C under the mean field approximation can be estimated by $T_C = 2\Delta E/(3k_B)$ according to the Heisenberg model[41], which is 235 K for NbTe₂ under -9% strain. So, NbTe₂ under -9% strain is paramagnetic at room temperature.

CONCLUSION

In summary, steep-slope transistors using cold metals as the injection source are proposed and investigated by quantum transport simulations. It is revealed that cold metals such as 2D TMDs of NbX₂ and TaX₂ can effectively cut off the Boltzmann tail of electrons due to the energy gap above the Fermi level. Therefore, sub-60 mV/decade switching can be obtained by using such cold metals as the injection source. Comprehensive device simulations show that a steep subthreshold swing (23 mV/decade) and high on-state current over $1.0 \times 10^3 \mu A/\mu m$ is achievable in both NbTe₂-MoSe₂ and NbTe₂-HfS₂ CS-FETs, which

exhibit promising performance with respect to the requirements of ITRS 2013 for both high-performance and low-power applications. Our findings pave a way for using cold metal materials to design steep slope electronic devices with the rapid development of emerging materials.

* Electronic address: feiliu@pku.edu.cn

- [1] A. C. Seabaugh, Q. Zhang, Low voltage tunnel transistors for beyond CMOS logic. *Proc. IEEE* **98**, 2095-2110 (2010).
- [2] A. M. Ionescu, H. Riel, Tunnel field-effect transistors as energy efficient electronic switches. *Nature* **479**, 329-337 (2011).
- [3] J. Appenzeller, Y. M. Lin, J. Knoch, P. Avouris, Band-to-band tunneling in carbon nanotube field-effect transistors. *Phys. Rev. Lett.*, **93**, 196805 (2004).
- [4] D. Sarkar, X. Xie, W. Liu, W. Cao, J. Kang, Y. Gong, S. Kraemer, P. M. Ajayan, K. Banerjee, K., A subthermionic tunnel field-effect transistor with an atomically thin channel. *Nature*, **526**, 91 (2015).
- [5] K. Gopalakrishnan, P. B. Griffin, and J. D. Plummer, Impact ionization MOS (I-MOS)-Part I: device and circuit simulations. *IEEE Trans. Electron Devices*. **52**, 69C76 (2005).
- [6] S. Salahuddin and S. Datta, Use of negative capacitance to provide voltage amplification for low power nanoscale devices. *Nano Lett.* **8**, 405-410 (2008).
- [7] F. Liu, C. G. Qiu, Z. Y. Zhang, L. Peng, J. Wang, Z. Wu, H. Guo, First principles simulation of energy efficient switching by source density of states engineering. *IEEE International Electron Devices Meeting (IEDM)*, 763-766 (2018).
- [8] F. Liu, C. Qiu, Z. Zhang, et al., Dirac electrons at the source: breaking the 60-mV/decade switching limit. *IEEE Trans. Electron Devices.*, **65**, 2736-2743 (2018).
- [9] C. Qiu, F. Liu, L. Xu, et al., Dirac source field-effect transistors as energy-efficient and high-performance electronic switches. *Science* **361**, 387 (2018).
- [10] D. Logoteta, M. G. Pala, J. Choukroun, P. Dollfus, G. Iannaccone, A steep-slope MoS₂-Nanoribbon MOSFET based on an intrinsic cold-contact effect. *IEEE Electron Device Lett.*

- 40**, 1550 (2019).
- [11] K. S. Novoselov, D. Jiang, F. Schedin, T. J. Booth, V. V. Khotkevich, S. V. Morozov, A. K. Geim, Two dimensional atomic crystals. *Proc. Natl Acad. Sci. USA*, **102** 10451-3 (2005).
- [12] X. Xi, Z. Wang, W. Zhao, J. H. Park, K. T. Law, H. Berger, L. Forro, J. Shan, K. F. Mak, Ising pairing in superconducting NbSe₂ atomic layers. *Nat. Phys.*, **12**, 139-143 (2015).
- [13] J. N. Coleman, M. Lotya, A. O'Neill, S. D. Bergin, P. J. King, U. Khan, K. Young, A. Gaucher, S. De, R. J. Smith, et al. Two-Dimensional Nanosheets Produced by Liquid Exfoliation of Layered Materials. *Science* **331**, 568C571 (2011).
- [14] R. J. Smith, P. J. King, M. Lotya, C. Wirtz, U. Khan, S. De, A. O'Neill, G. S. Duesberg, J. C. Grunlan, G. Moriarty, et al. Large-scale exfoliation of inorganic layered compounds in aqueous surfactant solutions. *Adv. Mater.* **23**, 3944-3948 (2011).
- [15] J. Wu, J. Peng, Z. Yu, Y. Zhou, Y. Guo, Z. Li, Y. Lin, K. Ruan, C. Wu, Y. Xie, Acid-assisted exfoliation toward metallic sub-nanopore TaS₂ monolayer with high volumetric capacitance. *J. Am. Chem. Soc.* **140**, 493-498 (2018).
- [16] H. Wang, X. Huang, J. Lin, J. Cui, Y. Chen, C. Zhu, F. Liu, Q. Zeng, J. Zhou, P. Yu, X. Wang, High-quality monolayer superconductor NbSe₂ grown by chemical vapour deposition. *Nature commun.* **8**, 394 (2017).
- [17] J. Zhou, J. Lin, X. Huang, Y. Zhou, Y. Chen, J. Xia, H. Wang, Y. Xie, H. Yu, J. Lei, D. Wu, A library of atomically thin metal chalcogenides. *Nature*, 556(7701), p.355-359 (2018).
- [18] J. Shi, X. Chen, L. Zhao, Y. Gong, M. Hong, Y. Huan, Z. Zhang, P. Yang, Y. Li, Q. Zhang, Q. Zhang, L. Gu, H. Chen, J. Wang, S. Deng, N. Xu, Y. Zhang, Chemical vapor deposition grown wafer-scale 2D tantalum diselenide with robust charge-density-wave order. *Adv. Mater.* **30**, 1804616 (2018).
- [19] M. Hossain, J. Wu, W. Wen, H. Liu, X. Wang, L. Xie, Chemical vapor deposition of 2D vanadium disulfide and diselenide and Raman characterization of the phase transitions, *Adv. Mater. Interfaces*, **5**, 1800528 (2018).
- [20] Y. Zhang, L. Yin, J. Chu, T. A. Shifa, J. Xia, F. Wang, Y. Wen, X. Zhan, Z. Wang, J. He, Edge-epitaxial growth of 2D NbS₂-WS₂ lateral metal-semiconductor heterostructures. *Adv. Mater.* **30**, 1803665 (2018).
- [21] Z. Zhang, P. Yang, M. Hong, S. Jiang, G. Zhao, J. Shi, Q. Xie, Y. Zhang, Recent progress in the controlled synthesis of 2D metallic transition metal dichalcogenides. *Nanotech.*, **30**,

- 182002 (2019).
- [22] M. M. Ugeda, A. J. Bradley, Y. Zhang, S. Onishi, Y. Chen, W. Ruan, C. Ojeda-Aristizabal, H. Ryu, M. T. Edmonds, H. Z. Tsai, A. Riss, S. K. Mo, D. Lee, A. Zettl, Z. Hussain, Z. X. Shen, M. F. Crommie, Characterization of collective ground states in single-layer NbSe₂. *Nat. Phys.* , **12**, 92-97 (2016).
- [23] X. X. Xi, H. Berger, L. Forro, J. Shan, K. F. Mak, Gate Tuning of Electronic Phase Transitions in Two-Dimensional NbSe₂. *Phys. Rev. Lett.* **117**, 106801 (2016).
- [24] Y. Cao, A. Mishchenko, G. L. Yu, E. Khestanova, A. P. Rooney, E. Prestat, A. V. Kretinin, P. Blake, M. B. Shalom, C. Woods, J. Chapman, G. Balakrishnan, I. V. Grigorieva, K. S. Novoselov, B. A. Piot, M. Potemski, K. Watanabe, T. Taniguchi, S. J. Haigh, A. K. Geim, R. V. Gorbachev, Quality heterostructures from two-dimensional crystals unstable in air by their assembly in inert atmosphere, *Nano Lett.*, **15**, 4914-4921 (2015).
- [25] G. Kresse, J. Furthmüller, Efficient iterative schemes for ab initio total-energy calculations using a plane-wave basis set. *Phys. Rev. B* **54**, 11169C11186 (1996).
- [26] P. E. Blöchl, Projector augmented-wave method. *Phys. Rev. B* **50**, 17953C17979 (1994).
- [27] G. Kresse, D. Joubert, From ultrasoft pseudopotentials to the projector augmented-wave method. *Phys. Rev. B* **59**, 1758C1775 (1999).
- [28] J. P. Perdew, K. Burke, M. Ernzerhof, Generalized gradient approximation made simple. *Phys. Rev. Lett.* **77**, 3865C3868 (1996).
- [29] S. Grimme, Semiempirical GGA-type density functional constructed with a long-range dispersion correction. *J. Comput. Chem.* **27**, 1787C1799 (2006).
- [30] J. Heyd, G. E. Scuseria, M. Ernzerhof, Hybrid functionals based on a screened Coulomb potential. *J. Chem. Phys.* **118**, 8207C8215 (2003).
- [31] J. Heyd, G. E. Scuseria, M. Ernzerhof, Erratum: Hybrid functionals based on a screened Coulomb potential. *J. Chem. Phys.* **124**, 219906 (2006).
- [32] S. Datta, *Quantum Transport: Atom to Transistor*. Cambridge, U.K.: Cambridge Univ. Press (2005).
- [33] J. Taylor, H. Guo, J. Wang, Ab initio modeling of quantum transport properties of molecular electronic devices, *Phys. Rev. B* **63**, 245407 (2001).
- [34] C. Zhang, C. Gong, Y. Nie, K. N. Min, C. Liang, Y. J. Oh, H. Zhang., W. Wang, S. Hong, L. Colombo, R. M. Wallace., K. Cho, Systematic study of electronic structure and band

- alignment of monolayer transition metal dichalcogenides in Van der Waals heterostructures, *2D Mater.* **4**, 4, 015026 (2017).
- [35] G. Liu, W. Shan, Y. Yao, W. Yao, D. Xiao, A three-band tight-binding model for monolayers of group-VIB transition metal dichalcogenides, *Phys. Rev. B*, **88**, 085433 (2013).
- [36] F. Liu, Y. Wang, X. Liu, J. Wang, H. Guo, Ballistic transport in monolayer black phosphorus transistors, *IEEE Trans. Electron Devices*, **61**, 3871-3876 (2014). 2014.2353213.
- [37] Process Integration, Devices, and Structures, (2013). Available: <http://www.itrs.net/>
- [38] S. Fang, R. K. Defo, S. N. Shirodkar, S. Lieu, G. A. Tritsarlis, and E. Kaxiras, Ab initio tight-binding hamiltonian for transition metal dichalcogenides, *Phys. Rev. B* **92**, 205108 (2015).
- [39] N. Marzari and D. Vanderbilt, Maximally localized generalized Wannier functions for composite energy bands, *Phys. Rev. B* **56**, 12847 (1997).
- [40] A. A. Mostofi, J. R. Yates, G. Pizzi, Y.-S. Lee, I. Souza, D. Vanderbilt, and N. Marzari, An updated version of WANNIER90: A tool for obtaining maximally-localised Wannier functions, *Comput. Phys. Commun.* **185**, 2309 (2014).
- [41] Y. Zhou, Z. Wang, P. Yang, X. Zu, L. Yang, X. Sun, F. Gao, Tensile strain switched ferromagnetism in layered NbS₂ and NbSe₂, *ACS Nano*, **6**, 6, 9727 (2012).